Santa Clara University
Scholar Commons

Electrical Engineering   School of Engineering

4-20-2009

Contact resistance in carbon nanostructure via interconnects

Wen Wu

Shoba Krishnan

Toshishige Yamada
Santa Clara University, tyamada@scu.edu

Xuhui Sun

Patrick Wilhite
Santa Clara University, pwilhite@scu.edu

See next page for additional authors

Follow this and additional works at: https://scholarcommons.scu.edu/elec

Recommended Citation

W. Wu, S. Krishnan, T. Yamada, X. Sun, P. Wilhite, R. Wu, K. Li, and C.Y. Yang, "Contact resistance in carbon nanostructure via interconnects," Applied Physics Letters 94, 163113 (3 pp) (2009). https://doi.org/10.1063/1.3123164

Authors

Wen Wu, Shoba Krishnan, Toshishige Yamada, Xuhui Sun, Patrick Wilhite, Raymond Wu, Ke Li, and Cary Y. Yang

Contact resistance in carbon nanostructure via interconnects

Wen Wu, Shoba Krishnan, Toshishige Yamada,[a] Xuhui Sun, Patrick Wilhite,
Raymond Wu, Ke Li, and Cary Y. Yang
Center for Nanostructures, Santa Clara University, Santa Clara, California 95053, USA

We present an in-depth electrical characterization of contact resistance in carbon nanostructure via interconnects. Test structures designed and fabricated for via applications contain vertically aligned arrays of carbon nanofibers (CNFs) grown on a thin titanium film on silicon substrate and embedded in silicon dioxide. Current-voltage measurements are performed on single CNFs using atomic force microscope current-sensing technique. By analyzing the dependence of measured resistance on CNF diameter, we extract the CNF resistivity and the metal-CNF contact resistance. © *2009 American Institute of Physics*. [DOI: 10.1063/1.3123164]

Recent process and reliability issues in state-of-the-art copper interconnects have driven researchers to actively seek alternative materials for next-generation on-chip interconnect technologies. Carbon nanotubes (CNTs) and carbon nanofibers (CNFs) are possible candidates that can withstand or even exceed the reliability standards of comparable copper systems.[1–3] Besides their superior current capacity, CNTs and CNFs exhibit robust thermal and mechanical properties.[4,5] To incorporate carbon-based interconnects into integrated circuit fabrication processes, one vital consideration is the controllable synthesis of carbon nanostructures. Carbon nanostructure growth depends on the key parameters governing the reaction, such as temperature, catalyst geometry, and gas flow rate, which affect to various degrees the performance of active devices fabricated in front-end processes. Moreover, such growth comes with formation of carbon-metal interfaces which must be optimized to achieve low contact resistances required by the International Technology Roadmap for Semiconductors.[6]

Imaging with microscopy, such as with scanning electron microscope (SEM) and scanning transmission electron microscopy, provides structural and compositional information of the nanoscale materials and their interfaces.[7] To study the structure-property relationships for these interfaces, so that the materials can potentially be incorporated in next-generation chip technologies, electrical characterization of their direct and alternate current (dc and ac) behaviors is essential. Such extensive measurements require development of robust test methodologies. Four-point-probe measurements minimize the voltage drop across contacts to extract intrinsic and contact resistances, and have been widely adopted for horizontal one-dimensional nanostructures.[8,9] However, it is challenging to fabricate the corresponding four-point test structures for vertical nanostructures such as vias due to complex three-dimensional nature of the electrode-via system. Therefore, finding an alternative way to extract contact resistance in a via structure is critically needed. Measured electrical characteristics of CNT vias have been reported,[10,11] but few articles focus on the differentiation of contact resistances from the overall via resistances. In this letter, we present resistance extraction methodology for

vertical one-dimensional nanostructures. Using this method, we can separate the interfacial or contact resistance from the intrinsic bulk resistance of nanostructures. To properly analyze the measurement results, a diameter-dependent contact resistance model is proposed, which agrees well with single-CNF measurements using atomic force microscope (AFM) current-sensing technique.

Figure 1(a) illustrates the cross-section of a CNF array used for electrical characterization. Details of the CNF-array test structure fabrication have been reported elsewhere.[12] The inherent vertical alignment of CNFs grown by plasma-enhanced chemical vapor deposition makes integration into planar silicon processing technologies feasible. In Fig. 1(a), the platinum coating on the surface of the AFM probe tip (tip radius <60 nm) forms a nanoscale electrical measurement probe. With the probe tip virtually grounded, a variable dc bias voltage is applied to the sample, and an amplifier in the controller senses the current flow through the sample. When the AFM probe scans the sample surface in contact mode, current distribution and surface topographies of the sample are obtained simultaneously. This allows the users to precisely probe individual CNFs protruding out of the oxide and measure their electrical characteristics. The SEM image (top view) of the sample surface is shown in Fig. 1(b). With a constant dc voltage applied between the scanning probe tip and the sample base electrode, surface topographic images can be obtained.

The surface topographic image obtained for each sample allows us to systematically locate single CNFs for current-voltage (*I-V*) measurements. For such characterization of
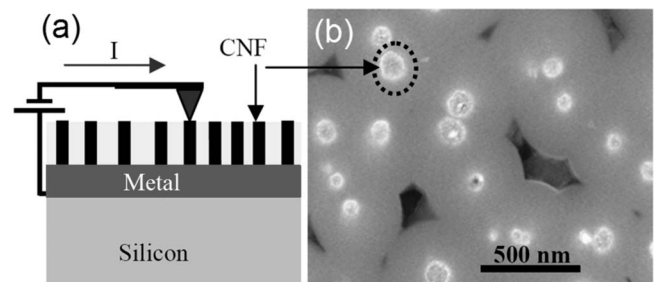

FIG. 1. (a) Cross-section of CNF arrays embedded in SiO$_2$ with a current-sensing AFM tip in contact mode, and (b) an SEM image of sample surface where a CNF protruding out of oxide is highlighted by a dashed circle.

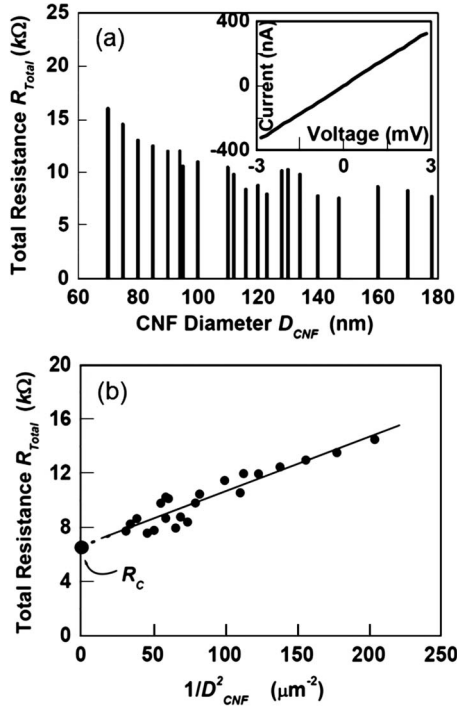[a]Author to whom correspondence should be addressed. Electronic mail: tyamada@scu.edu.

FIG. 2. Measured total resistance as a function of (a) D_{CNF}, where the inset shows a typical *I-V* curve of a single (b) $1/(D_{CNF})^2$ and its linear fit, yielding R_C.

nanostructures, it is necessary to apply a low current or voltage to the device under test by sweeping the dc bias voltages between −3 and +3 mV. The inset in Fig. 2(a) shows a linear *I-V* behavior obtained from AFM measurement for one CNF of diameter $D_{CNF}=120$ nm. *I-V* measurements were carried out on several CNFs of varying diameters with nearly constant length L_{CNF}. These measurements are plotted as a function of D_{CNF} in Fig. 2(a).

The resistance (R_{tot}) obtained from the measured *I-V* curves consists of the CNF bulk resistance (R_{CNF}) in series with the total contact resistance (R_C), or $R_{tot}=R_C+R_{CNF}$, where R_C represents the sum of CNF-metal and probe tip-CNF contact resistances. The contact resistance between the Pt probe tip and the CNF is dependent on the pressure applied on the tip, which can be minimized empirically. Since classical or Ohmic transport prevails in this case, R_{CNF} can be expressed as $R_{CNF}=4\rho_{CNF}L_{CNF}/\pi D_{CNF}^2$, where ρ_{CNF} is the CNF resistivity.

In macroscale, R_C is expected to be inversely proportional to the contact area. However, our data indicate a somewhat different dependence of R_C on D_{CNF}. In fact, we have previously demonstrated that tunneling is the dominant transport mechanism between a CNT tip and electrode,[13] which is similar to our present CNF-metal interface. If the tunneling barrier thickness w has a certain correlation with D_{CNF} such that w is thicker for larger D_{CNF}, then R_C can be independent of D_{CNF}. This is because tunneling resistance is proportional to $4/(\pi D_{CNF}^2)\exp(2\alpha w)$, where α is the decay constant of an electron wave function in the barrier.[13] If $\alpha w \sim \ln(D_{CNF})$, then the tunneling resistance can be almost constant. When the interface asperity is significant, as expected for the as-grown contact between CNF and electrode, the effective w for tunneling tends to be larger for larger D_{CNF}, making the constant R_C assumption a reasonable starting point for our data analysis. Accordingly,

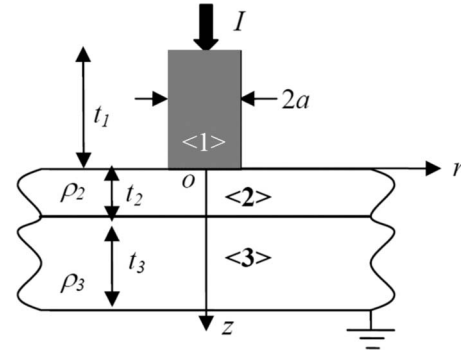FIG. 3. Geometry of a cylindrical contact between a conductor ($\langle 1 \rangle$) and a thin poorly conducting layer ($\langle 2 \rangle$) on a metal substrate ($\langle 3 \rangle$).

$$R_{tot} = R_C + R_{CNF} \equiv c_0 + \frac{4\rho_{CNF}L_{CNF}}{\pi D_{CNF}^2}. \tag{1}$$

Thus, plotting R_{tot} versus $1/(D_{CNF})^2$ and extrapolating to $1/(D_{CNF})^2 \to 0$ (i.e., $R_{CNF} \to 0$) yields constant R_C or c_0. The measured R_{tot} as a function of $1/(D_{CNF})^2$ for twenty-two 4.5 μm long devices is shown in Fig. 2(b). The extracted c_0 is 6.4 kΩ with an error bar of about 400 Ω, and the resulting ρ_{CNF} is 7.3×10^{-4} Ω cm.

Next we consider the possibility where R_C depends on D_{CNF}. Figure 3 shows a cylindrical conductor (region $\langle 1 \rangle$) corresponding to CNF with radius a and height t_1 (=CNF length L_{CNF}) in contact with a two-layer substrate. We assume the existence of a thin poorly conducting layer (region $\langle 2 \rangle$), e.g., interfacial oxide or contaminated layer, between the CNF and metal electrode (region $\langle 3 \rangle$) formed during CNF growth. These layers, in addition to the tunneling barrier described above, represent the main source of contact resistance, as the upper contact resistance (probe tip CNF) is relatively small compared to the base contact resistance. The thicknesses of region $\langle 2 \rangle$ and region $\langle 3 \rangle$ are t_2 and t_3, with resistivities ρ_2 and ρ_3, respectively.

We now proceed to determine the resistance R'_C describing the transport across these layers. To analyze the potential distribution in regions $\langle 2 \rangle$ and $\langle 3 \rangle$, the Poisson equation $\nabla^2 \varphi_i = 0$ in the cylindrical coordinate in Fig. 3 is solved for $i=2$ and 3 with the boundary conditions $\varphi_2(r, z=0) = V_0$ for $r \le a$ and $\varphi_3(r, z=t_2) = 0$ for any r. Solution can be obtained using Hankel transform,[14,15] and the total current is expressed by $I = \int(1/\rho)(-\partial\varphi/\partial z)2\pi r dr$.[14] Then, $R'_C = V_0/I$. For $\rho_2 \ne \rho_3$ and a thin interfacial layer $0 < t_2/a \le 0.1$, R'_C can be expressed as $R'_C = \rho_3/4a + \rho_2 t_2(1-\rho_3^2/\rho_2^2)/\pi a^2$.[16] In our case, $D_{CNF}=2a$ ranges between 70 and 180 nm and t_2 is typically much shorter.[17] Thus $t_2/a \ll 1$ holds true in practice, and since $\rho_2 > \rho_3$ in general, the solution yields $R'_C \sim \rho_3/4a$.

The foregoing analysis suggests that the total contact resistance R_C has a diameter-dependent component in addition to the constant tunneling resistance discussed above. Thus, $R_C(D_{CNF}) = c_1 + c_2/D_{CNF}$ and R_{tot} is given by

$$R_{tot} = R_C(D_{CNF}) + R_{CNF} \equiv c_1 + \frac{c_2}{D_{CNF}} + \frac{4\rho_{CNF}L_{CNF}}{\pi D_{CNF}^2}. \tag{2}$$

Using Eq. (2), we have extracted $c_1=5.4$ kΩ, $c_2=2.58 \times 10^{-2}$ Ω cm, and $\rho_{CNF}=4.30 \times 10^{-4}$ Ω cm from the same measurement results. Comparison of the modeling results (denoted by the solid line) with the measurement is given in
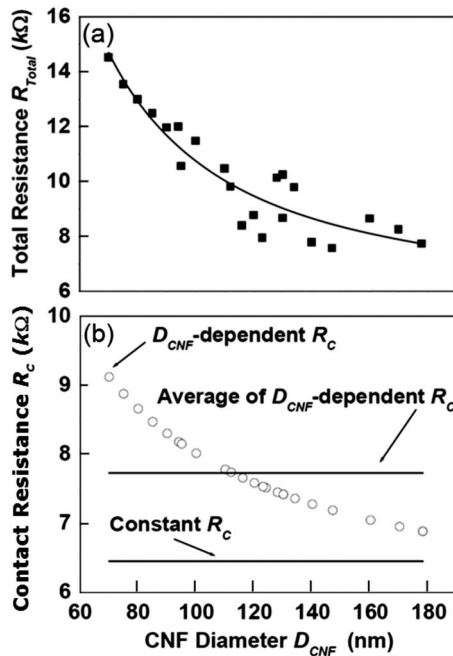
FIG. 4. (a) Measured resistances (solid squares) and corresponding modeling results (solid line) vs D_{CNF}. (b) Modeled contact resistances vs D_{CNF}. Two solid lines represent average contact resistances derived based on constant-R_C and diameter-dependent-R_C assumptions, respectively.

Fig. 4(a). Note that this model yields $\rho_3 = 5 \times 10^{-2}$ Ω cm, which is considerably higher than that of Ti, the substrate metal in contact with CNF. This discrepancy underscores the limitation of this model in describing transport behavior outside the interfacial region. Moreover, the complexity of the interfacial layer between CNF and Ti renders the assumption of an ideal contact between regions ⟨2⟩ and ⟨3⟩ rather approximate. Nevertheless, the model represents a first-order correction to the diameter-independent assumption described above.

Figure 4(b) shows the extracted $R_C(D_{\text{CNF}})$ using Eq. (2). $R_C(D_{\text{CNF}})$ is 4.3 kΩ at $D_{\text{CNF}} = 60$ nm, and is 1.4 kΩ at $D_{\text{CNF}} = 180$ nm, with an average $R_C(D_{\text{CNF}})$ of 7.7 kΩ. Unlike the low-resistance behavior exhibited by metal contacts, $R_C(D_{\text{CNF}})$ values obtained here are at least two times larger than R_{CNF} of carbon nanofibers with similar diameters. $R_C(D_{\text{CNF}})$ therefore dominates the electrical characteristics of carbon nanostructures in via interconnects. The figure also shows the extracted R_C when assumed constant. Compared to $R_C(D_{\text{CNF}})$, which seems to approach the constant R_C value for large D_{CNF}, the constant assumption is clearly an underestimate (and probably the lower limit for large D_{CNF}) as it ignores current crowding at the interface for smaller D_{CNF}. Nevertheless, for the CNF via interconnects studied here, the constant-R_C assumption provides a quick and simple estimation of contact resistances.

The AFM current-sensing technique enables us to probe individual CNFs and obtain *I-V* curves for single nanofibers. We extract the CNF bulk resistivity and contact resistance from the total resistance measurements using two separate assumptions, constant R_C and diameter-dependent $R_C(D_{\text{CNF}})$. We find that the constant assumption leads to an underestimate of the contact resistance, while assuming reciprocal-diameter dependence of $R_C(D_{\text{CNF}})$ is justified both theoretically and empirically. Our results also show that the contact resistance at the metal-carbon interface dominates the electrical characteristics of carbon nanostructures in via interconnects. The contact resistance extraction methodology presented here, based on varying diameters, is applicable to other one-dimensional nanostructures.

[1] Z. Yao, C. L. Kane, and C. Dekker, Phys. Rev. Lett. **84**, 2941 (2000).
[2] B. Q. Wei, R. Vajtai, and P. M. Ajayan, Appl. Phys. Lett. **79**, 1172 (2001).
[3] A. Javey, P. Qi, Q. Wang, and H. Dai, Proc. Natl. Acad. Sci. U.S.A. **101**, 13408 (2004).
[4] Q. Ngo, T. Yamada, M. Suzuki, Y. Ominami, A. M. Cassell, J. Li, M. Meyyappan, and C. Y. Yang, IEEE Trans. Nanotechnol. **6**, 688 (2007).
[5] M. Suzuki, Y. Ominami, Q. Ngo, C. Y. Yang, A. M. Cassell, and J. Li, J. Appl. Phys. **101**, 114307 (2007).
[6] International Technology Roadmap for Semiconductors—Interconnect, available at http://www.itrs.net/Links/2007ITRS/2007_Chapters/2007_Interconnect.pdf.
[7] Nanotechnology Measurement Handbook, available at http://www.keithley.com/news/prod040507.
[8] A. Bachtold, M. Henny, C. Terrier, C. Strunk, C. Schonenberger, J. P. Salvetat, J. M. Bonard, and L. Forro, Appl. Phys. Lett. **73**, 274 (1998).
[9] A. S. Walton, C. S. Allen, K. Critchley, M. L. Gorzny, J. E. McKendry, R. M. D. Brydson, B. J. Hickey, and S. D. Evans, Nanotechnology **18**, 065204 (2007).
[10] A. Kawabata, S. Sato, T. Nozue, T. Hyakushima, M. Norimatsu, M. Mishima, T. Murakami, D. Kondo, K. Asano, M. Ohfuti, H. Kawarada, T. Sakai, M. Nihei, and Y. Awano, Proceedings of the IEEE International Interconnect Technology Conference (IITC), Burlingame, CA, 2008, p. 237.
[11] J. C. Coiffic, M. Fayolle, H. Le Poche, S. Maitrejean, and S. Olivier, Proceedings of the IEEE International Interconnect Technology Conference (IITC), Burlingame, CA, 2008, p. 153.
[12] W. Wu, D. Nguyen, P. Wilhite, T. Saito, S. Krishnan, and C. Y. Yang, Proceedings of 8th IEEE Conference on Nanotechnology (Nano '08), Arlington, TX, 2008, p. 300.
[13] T. Yamada, Appl. Phys. Lett. **78**, 1739 (2001).
[14] R. Holm, *Electronic Contacts: Theory and Application* (Springer, New York, 1967).
[15] M. W. Denhoff, J. Phys. D: Appl. Phys. **39**, 1761 (2006).
[16] J. R. Dryden, ASME J. Heat Transfer **105**, 408 (1983).
[17] T. Yamada, M. Suzuki, H. Kitsuki, T. Saito, D. Fabris, X. Sun, P. Wilhite, and C. Y. Yang, Proceedings of 8th IEEE Conference on Nanotechnology (Nano '08), Arlington, TX, 2008, p. 263.